Available online at www.sciencedirect.com
SCIENCE DIRECT®
Bioorganic & Medicinal Chemistry 14 (2006) 352–365
Bioorganic & Medicinal Chemistry

Quantitative structure–activity relationships for small non-peptide antagonists of CXCR2: Indirect 3D approach using the frontal polygon method

Andrei I. Khlebnikov,[a,*] Igor A. Schepetkin[b] and Mark T. Quinn[b,*]

[a]*Department of Chemistry, Altai State Technical University, Barnaul 656099, Russia*
[b]*Department of Veterinary Molecular Biology, Montana State University, Bozeman, MT 59717, USA*

Received 26 July 2005; accepted 8 August 2005
Available online 22 September 2005

Abstract—The chemokine receptor, CXCR2, plays an important role in recruiting granulocytes to sites of inflammation and has been proposed as an important therapeutic target. A number of CXCR2 antagonists have been synthesized and evaluated; however, quantitative structure–activity relationship (QSAR) models have not been developed for these molecules. Most CXCR2 antagonists can be grouped into four related categories: *N*,*N*′-diphenylureas, nicotinamide *N*-oxides, quinoxalines, and triazolethiols. Based on these categories, we developed a QSAR model for 59 nonpeptide antagonists of CXCR2 using a partial 3D comparison of the antagonists with local fingerprints obtained from rigid and flexible fragments of the molecules. Each compound was represented by calculated structural descriptors that encoded atomic charge, molar refraction, hydrophobicity, and geometric features. We obtained good conventional R^2 coefficients, high leave-one-out cross-validated values for the whole dataset ($R^2_{cv} = 0.785$), as well as for the dataset divided into subsets of triazolethiol derivatives ($R^2_{cv} = 0.821$) and joint subset of *N*′-diphenylureas, nicotinamide *N*-oxides, *N*,*N*′-diphenylureas, and quinoxaline derivatives and quinoxalines derivatives ($R^2_{cv} = 0.766$), indicating a good predictive ability and robustness of the model. Additionally, charge distribution was found to be a significant contributor in modeling whole dataset. Using our model, structural fragments (submolecules) responsible for the antagonist activity were also identified. These data suggest the QSAR models developed here may be useful in guiding the design of CXCR2 antagonists from molecular fragments.

1. Introduction

Leukocyte recruitment is mediated through the actions of both exogenous and endogenous chemotactic factors.[1] Among the primary endogenous chemotactic factors are the chemokines or chemoattractant cytokines.[2] Chemokines belong to a large superfamily of small (8–10 kDa), structurally related proteins that are characterized by a distinctive pattern of four conserved cysteines.[3] One family of chemokines is characterized by the presence of an intervening amino acid between the first pair of conserved cysteines and is known as the 'Cys-X-Cys' (CXC) or α chemokine family. The CXC chemokines can be further subdivided into two groups, one containing a glutamate–leucine–arginine (ELR) motif between the N-terminus and the first cysteine and the other without this motif.[3] The ELR-containing CXC chemokines, such as interleukin-8 (IL-8) and growth-related oncogene α (Gro-α), play important roles in the recruitment and activation of neutrophils during inflammation.[2] Indeed, these chemokines have been implicated in the pathogenesis of a number of inflammatory diseases, including asthma, rheumatoid arthritis, psoriasis, reperfusion injury, and adult respiratory distress syndrome.[4,5] Furthermore, the ELR-containing CXC chemokines are potent promoters of angiogenesis and mediate their angiogenic activity via binding and activating specific surface receptors on the endothelium.[6] In certain cases, the angiogenic activity of these chemokines can also contribute to tumorigenesis.[7]

Physiological responses to ELR-containing CXC chemokines are mediated via two distinct transmembrane G-protein-coupled receptors, known as CXC receptors 1 and 2 (CXCR1 and CXCR2, respectively).[8] CXCR1

Keywords: CXCR2 antagonists; QSAR; Frontal polygons; Molecular descriptors; Drug design; Molecular modeling.
* Corresponding authors. Tel.: +7 3852 245513/+7 3852 522436; fax: +7 3852 367864 (A.I.K); tel.: +1 406 994 5721; fax: +1 406 994 4303 (M.T.Q); e-mail addresses: aikhlebnikov@narod.ru; mquinn@montana.edu

0968-0896/$ - see front matter © 2005 Elsevier Ltd. All rights reserved.
doi:10.1016/j.bmc.2005.08.026

binds IL-8 and granulocyte chemotactic protein-2 (GCP-2/CXCL6) with high affinity, whereas CXCR2 is promiscuous, binding seven known ELR α-chemokines with high affinity, including GRO-α (CXCL-1), GRO-β (CXCL-2), GRO-γ (CXCL-3), epithelial neutrophil activating peptide 78 (ENA-78/CXCL-5), GCP-2 (CXCL-6), neutrophil-activating peptide-2 (NAP-2/CXCL-7), and IL-8 (CXCL-8).[8] Furthermore, CXCR2 is expressed on a wide range of cell types, such as neutrophils, mast cells, T cells, keratinocytes, and cerebellar neurons.[9–11]

Studies with $CXCR2^{-/-}$ mice demonstrated that CXCR2 plays an essential role in neutrophil recruitment during inflammatory responses.[12,13] Additionally, marked reduction in the spontaneous metastases of tumor cells to the lungs was observed in $CXCR2^{-/-}$ mice.[7] Thus, CXCR2 has been proposed as an important target for drug development, as such therapeutic agents would be useful in the treatment of a number of diseases. Indeed, CXCR2 is one of the first chemokine receptors for which a potent, small-molecule antagonist (SB225002) was developed as a potential treatment for inflammatory diseases, such as rheumatoid arthritis, chronic obstructive pulmonary disease, bronchopulmonary dysplasia, and retrovirus infections.[14–16] Subsequently, many chemically diverse small molecule CXCR2 antagonists have been reported.[17–22] Thus, CXCR2 antagonists are considered an exciting alternative for the development of beneficial therapeutics with antiinflammatory and, possibly, anticancer effects.

Construction of quantitative structure–activity relationship (QSAR) models is essential for understanding the molecular mechanism of action of receptor antagonists, their design, and virtual screening.[23] Among the known antagonists of chemokine receptors, this type of analysis has been performed only for CCR5 synthetic antagonists,[24–26] and, to our knowledge, there are no reported QSAR models for CXCR2 antagonists. Currently, several QSAR models utilizing a flexible docking approach have been shown to be highly efficient in the description of ligand–receptor interactions.[27] Alternative approaches utilize ligand-based 3D-QSAR principles and are applicable when a detailed receptor structure is not available. These methods rely on pair-wise comparison of molecular spatial structures within a dataset or their superimposition on a template molecule.[28] The problems of conformational flexibility and structural diversity emerge immediately on performing structure comparisons when a data set includes molecules from different chemical classes. Although several approaches for resolving these problems have been suggested,[29,30] there are still significant difficulties in defining optimal orientation and/or conformation of a compound with respect to a given template.

The approach used in the present study exploits the hypothesis of local similarity, which allows us to circumvent these difficulties by using a frontal polygon method.[31,32] We utilized this approach to investigate the structure–activity relationships of the CXCR2-antagonists, and the partial 3D comparison of antagonists with local 'fingerprints' obtained from molecules of the most and least active compounds in the dataset was used to construct QSAR models. These models provide a basis for further application in activity prediction of newly designed antagonists and virtual drug screening.

2. Results

Ligand-based QSAR and drug design by the frontal polygon method is characterized by a large array of optimal superimpositions (OS). The following values of weight coefficients were used during formation of such arrays: $w_r = 11.86$, $w_h = 2.40$, $w_q = 3.28$, $w_H = 0.132$, and $w_R = 3.05 \cdot 10^{-4}$. These coefficients were calculated according to Eq. 2, with recognition criteria dispersions D determined through all compounds **1**–**59**. The number of OS (N_{OS}) increases significantly with the decrease of selection control when the K_0 value is enhanced. In the case of $K_0 = 1$, the sum F of weighed squares for deviations of recognition parameters in Eq. 1 is equal to the weighted dispersion of these parameters within a dataset, i.e., low-specific superimpositions can be treated as optimal. With lower K_0 values, higher specificity is necessary for a superimposition to become optimal, and the N_{OS} of the OS array becomes smaller. The relationship between N_{OS} values and K_0 for some antagonists investigated is shown in Figure 1. With increasing K_0 from 0.1 to 0.5, the N_{OS} value was enhanced by 20–50 times. This leads to changes in the quality of QSAR models, as is discussed below.

Some of the template fingerprints have a rather high percent participation in OS (Table 1). Clearly, these fingerprints reflect the most common structural features of compounds in a given dataset in terms of geometry, charge distribution, hydrophobicity, and size of substituents. The phenyl group and halogen-containing aromatic fragments are key examples of parent submolecules for these fingerprints. Fingerprints with

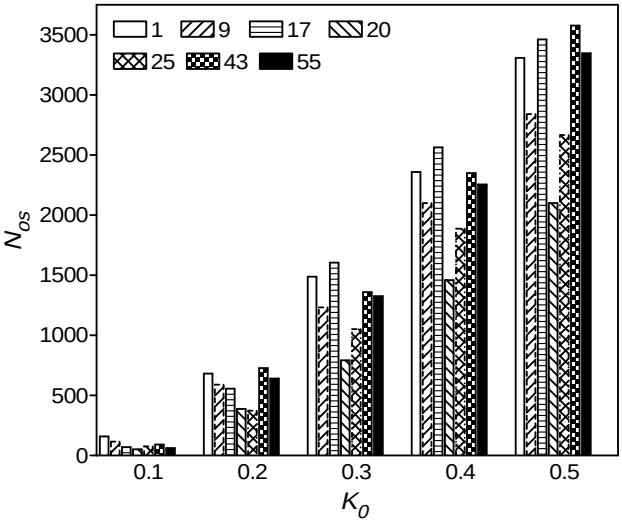

Figure 1. Relationship between numbers of optimal superimpositions (N_{OS}) and optimality criterion threshold (K_0) for selected compounds.

Table 1. Fractions of OS for selected template submolecules

Template submolecule (compound number in parentheses)	OS fraction (%)[a]
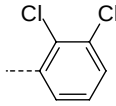 (**16**)	13.0
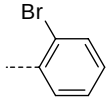 (**8**)	12.6
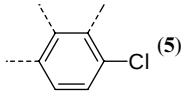 (**5**)	9.1
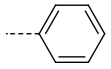 (**30**)	7.3
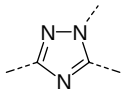 (**30**)	3.6
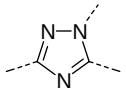 (**29**)	1.6
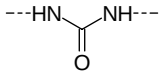 (**5**)	1.0
CF_3 (**31**)	0.03

[a] Percent values reflect the ratio of OS number with participation of a given submolecule to total OS number for Set 1+2.

low participation in OS are also present and were accounted for in deriving QSAR because differences in biological activity can be connected with subtle details of molecular structure. Moreover, it is noticeable from Table 1 that important triazole and carbamide submolecules represent contributed lower fractions of OS, although these fragments possess specific charge distributions and can participate significantly in molecular recognition.

The OS array obtained for each dataset was used for the construction of assignment matrix **V** of $N \times K$ size, where N is the number of compounds and K is the total number of atomic projections in all the template fingerprints. The matrix element V_{jk} is defined as the sum of projections assigned to the kth projection in all OS of the jth compound. The following dimensions of **V** matrices were obtained for the datasets: 27×246 (Set 1), 29×253 (Set 2), and 56×218 (Set 1+2). Matrices **V** are redundant (i.e., $N < K$), and their use for QSAR-analysis is possible only after reduction of space, which is achieved by applying the partial least-squares (PLS) procedure.[33] This reduction leads to a small basis of H variables, nevertheless reflecting the main part (P_{inf}) of the information contained in initial redundant matrices.

Characteristics of linear QSAR models (Eq. 4) derived with reduced basis for three datasets are shown in Table 2. The basis size $H = 5$ was chosen for Set 1 and Set 2, whereas better results were obtained for Set 1+2 with $H = 6$. If the number of variables (H) was smaller, then linear models with higher standard deviations (S) and lower correlation coefficients (R) were observed. Values of R^2_{cv} and P_{inf} also decreased. For example, the values $R = 0.877$, $R^2_{cv} = 0.712$, and $P_{inf} = 0.938$ were obtained if five variables were used for deriving QSAR. On the other hand, a larger basis size of $H > 6$ resulted in negligible improvement of the QSAR models.

The influence of K_0 on the quality of QSAR models is evident in Table 2. For each dataset, the R and R^2_{cv} values first become higher, reaching a maximal level, and then are lowered with the increase in K_0. This observation can be interpreted in terms of OS specificity. At $K_0 = 0.1$, when only OS with very high specificity are included in the array, a lot of structural information useful for better QSAR is lost, and the quality of linear models is not great. On the other hand, a loosened approach to OS selection at higher K_0 also decreases coefficients R and R^2_{cv} because of informational 'noise' (i.e., OS array contains low-specific superimpositions which do not reflect actual peculiarities of ligand recognition). Optimal QSAR models were constructed with $K_0 = 0.2$ for Set 1 and Set 2, and with $K_0 = 0.4$ for Set 1+2 (Table 2). Correlation coefficients >0.9 were achieved in these cases. Leave-one-out control of predictivity for three optimal QSAR equations is characterized by R^2_{cv} values >0.75. The especially high cross-validation coefficient of 0.821 for Set 2 can be explained by the low diversity of the dataset, which contained only triazolethiol molecules. It should be noted that

Table 2. Characteristics of QSAR models obtained for Set 1, Set 2, Set 1+2 of CXCR2 antagonists with different optimality criterion thresholds K_0

Dataset	K_0	S^2	R	R^2_{cv}	P_{inf}
Set 1	0.1	0.160	0.890	0.610	0.967
	0.2	**0.127**	**0.914**	**0.766**	**0.966**
	0.3	0.197	0.862	0.238	0.969
Set 2	0.1	0.113	0.853	0.611	0.953
	0.2	**0.048**	**0.940**	**0.821**	**0.898**
	0.3	0.060	0.926	0.794	0.900
Set 1+2	0.1	0.216	0.864	0.680	0.950
	0.2	0.175	0.891	0.737	0.946
	0.3	0.201	0.874	0.705	0.952
	0.4	**0.150**	**0.908**	**0.785**	**0.950**
	0.5	0.191	0.881	0.722	0.945

Optimal base QSAR models are indicated in bold.

Table 3. Calculated and cross-validated biological activities of CXCR2 antagonists

Compound	pIC_{50}	Set 1		Set 2		Set 1+2	
		$pIC_{50}^{(c)}$	$pIC_{50}^{(pred)}$	$pIC_{50}^{(c)}$	$pIC_{50}^{(pred)}$	$pIC_{50}^{(c)}$	$pIC_{50}^{(pred)}$
1	6.043	6.00	5.97			6.78	6.83
2	7.201	6.95	6.90			7.63	7.65
3	8.000	7.52	7.48			7.67	7.65
4	6.943	7.45	7.49			7.33	7.35
5	8.155	7.70	7.68			8.28	8.29
6	7.921	7.92	7.92			8.14	8.17
7	7.602	7.48	7.46			7.20	7.18
8	8.222	8.42	8.47			7.99	7.96
9	7.658	7.81	7.83			7.74	7.75
10	7.244	7.40	7.42			7.44	7.45
11	7.658	7.28	7.26			7.59	7.58
12	6.495	6.47	6.46			5.93	5.85
13	6.066	6.08	6.08			5.83	5.80
14	4.963	5.66	5.83			5.31	5.40
15	6.699	6.35	6.20			6.16	6.11
16	8.032	8.03	8.03			7.81	7.77
17	7.495	8.03	8.11			7.50	7.50
18	6.886	6.62	6.59			6.23	6.09
19	6.886	6.54	6.50			6.43	6.35
20	6.398	6.57	6.59			6.36	6.35
21	6.337	6.74	6.80			6.89	7.00
22	7.046	6.71	6.59			6.94	6.91
23	7.495	7.20	7.11			6.74	6.69
24	6.553	6.93	7.10			6.23	6.21
25	6.000	5.97	5.96			6.43	6.47
26	6.796	6.94	7.00			6.83	6.86
27	7.553	7.58	7.69			7.52	7.45
28	5.620			5.75	5.76	5.61	5.61
32	5.357			5.38	5.39	5.70	5.72
33	5.114			4.90	4.84	5.35	5.37
34	5.377			5.29	5.25	5.88	5.93
35	5.456			5.43	5.42	5.70	5.71
36	5.456			5.60	5.61	5.77	5.78
37	5.553			5.38	5.36	5.63	5.63
38	5.638			5.37	5.34	5.90	5.91
39	5.699			5.82	5.86	5.77	5.77
40	5.699			5.73	5.76	5.32	5.29
41	5.854			6.00	6.01	5.67	5.67
42	5.854			5.83	5.83	5.98	5.98
43	6.000			6.27	6.30	5.91	5.91
44	6.051			5.82	5.80	5.96	5.96
45	6.081			6.30	6.33	5.63	5.61
46	6.097			6.10	6.10	6.75	6.77
47	6.174			6.40	6.44	6.63	6.64
48	6.347			6.65	6.72	6.24	6.24
49	6.387			6.49	6.50	6.14	6.14
50	6.456			6.29	6.25	6.20	6.19
51	6.456			6.38	6.37	6.80	6.81
52	5.000			5.23	5.34	5.43	5.48
53	5.377			5.66	5.69	5.95	5.98
54	6.137			6.06	6.06	6.06	6.06
55	6.347			5.98	5.89	6.38	6.38
56	6.523			6.63	6.68	6.25	6.21
57	6.770			6.61	6.50	6.82	6.85
58	7.036			6.95	6.92	6.69	6.66
59	7.553			7.11	6.94	6.70	6.57

low-dimensional bases of H variables reproduce well the informational content of initial redundant **V** matrices, as indicated by P_{inf} values in Table 2.

Calculated and cross-validated activities of CXCR2 antagonists are shown in Table 3, and corresponding plots of cross-validated vs. experimental biological data are shown in Figure 2. For compounds from all three datasets, sufficiently small deviations of calculated $pIC_{50}^{(c)}$ and cross-validated $pIC_{50}^{(pred)}$ activities from the experimental pIC_{50} were obtained. Standard deviations of $pIC_{50}^{(c)}$ for Set 1, Set 2, and Set 1+2 were 0.356,

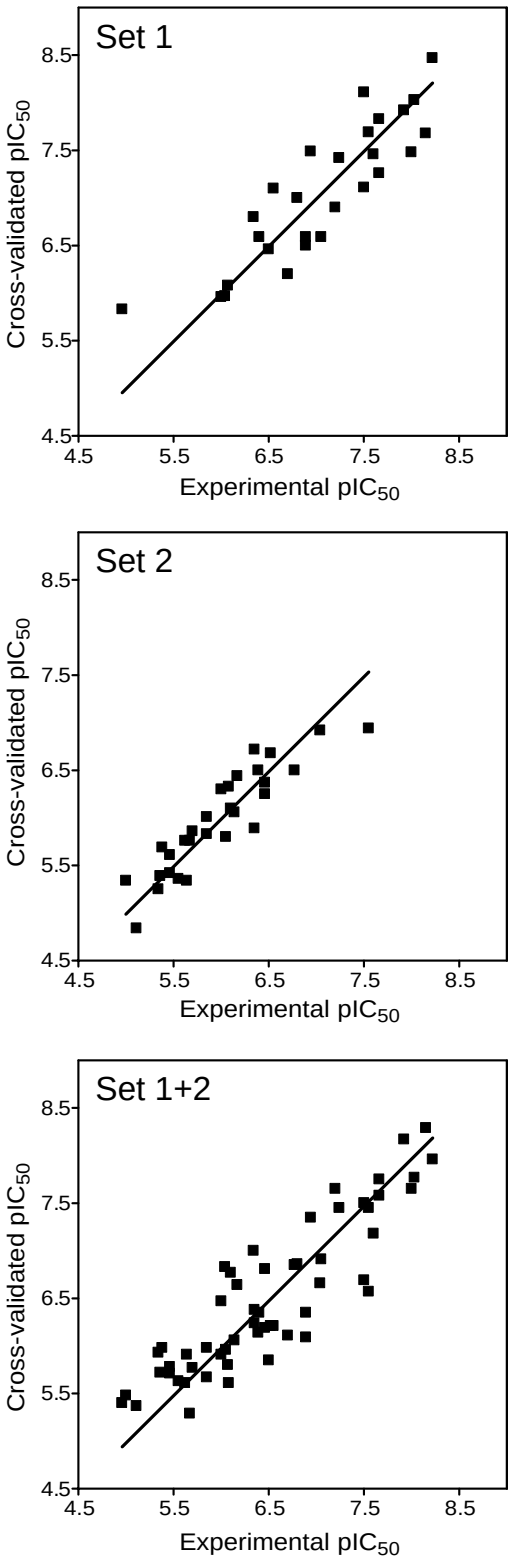

Figure 2. Comparison of cross-validated and experimentally determined biological activities for CXCR2 antagonists. Analysis was performed on compounds from Set 1, Set 2, and Set 1+2.

0.219, and 0.387, respectively, and corresponding values for $pIC_{50}^{(pred)}$ were of the same order of magnitude: 0.426, 0.321, and 0.432. Thus, the frontal polygon method allows us to derive high-quality QSAR models, both within structurally similar CXCR2 antagonists (Set 2), and within a more diverse series of compounds (Set 1 and Set 1+2).

Previously, we reported further improvements of QSAR models could be made by variations of weight coefficients in Eq. 1 and construction of higher-quality linear regressions related with new OS arrays.[35] Considering that each of these coefficients reflects an influence of certain recognition parameters on the magnitude of F in Eq. 1, we can assess the extent to which a given parameter is involved into molecular recognition process. Thus, we compared the quality of the base QSAR model for Set 1+2 (see Table 3 and the corresponding bold line in Table 2) with that of modified models derived after variation in one of the weight coefficients w_q, w_H, w_R (Table 4). This variation involved a 50% increase or decrease in one of these coefficients. Taking into account that summation of 5 terms is performed in Eq. 1, the K_0 value was also increased or decreased by 10% with respect to the initial value of $K_0 = 0.4$ in order to maintain the optimality criterion scale used in the base model. Data in Table 4 show that an improvement occurs only when w_q is enhanced. All variations of other weight coefficients lead to QSAR of lesser quality, as compared to the base model. Growth of R and R^2_{cv} with the increase of w_q may indicate that charge distribution plays a more important role than other factors in molecular recognition of CXCR2 antagonists during interaction with the receptor. Thus, CXCR2 ligand binding may involved charge transfer between phenyl rings and counterparts in the receptor, as well as localized electrostatic interactions P.[36,37]

3. Discussion

In this study, we utilized the frontal polygon method to develop QSAR models for 59 CXCR2 antagonists. Each rigid submolecule of the antagonists investigated was described by weight W_{jl} according to Eq. 6.[32] This additive characteristic allows evaluation of the biological activity of a compound as the sum of W_{jl} contributed by all of its fragments. In the approach described previously,[32] it was assumed that W_{jl} reflected an increment of activity for lth submolecule in a novel compound if this submolecule was surrounded by substituents similar in recognition parameters to the substituents surrounding a given submolecule in the parent compound. Thus, the fragment environment represents an important

Table 4. Characteristics of QSAR models obtained after 50% variation of weight coefficients w_q, w_H, w_R with respect to the base model for Set 1+2

QSAR model	S^2	R	R^2_{cv}	P_{inf}
Base model	0.150	0.908	0.785	0.950
Decreased w_q	0.197	0.877	0.709	0.939
Increased w_q	**0.128**	**0.922**	**0.793**	**0.956**
Decreased w_R	0.179	0.889	0.740	0.951
Increased w_R	0.151	0.907	0.780	0.948
Decreased w_H	0.182	0.887	0.731	0.956
Increased w_H	0.152	0.906	0.781	0.939

Table 5. Characteristics of rigid submolecules and their increments in CXCR2 inhibitory activity

Submolecule[a]	R_X	H_X	R_Y	H_Y	R_Z	H_Z	W_{jl}
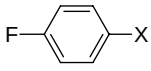	71.6	0.52					6.80
	55.7	−0.54					6.70
	79.6	1.12					3.69
8 fragments	75.1	1.18					3.59
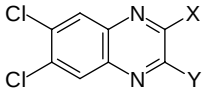	45.1	1.01	50.3	2.00			6.28
	45.1	1.01	33.6	1.76			3.59
2 fragments							
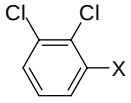	64.8	−0.24					5.44
	54.4	2.29					3.08
2 fragments							
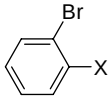	72.5	−0.09					5.40
	64.8	−0.24					5.14
	47.2	1.25					3.62
13 fragments	54.4	2.29					3.13
	55.4	2.24					5.08
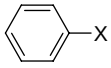	35.0	1.24					4.84
	52.6	−0.04					2.45
40 fragments	90.4	5.66					2.40
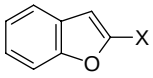	90.5	2.16					3.98
1 fragment							
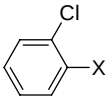	59.4	3.04					3.71
	54.4	2.29					3.55
2 fragments							
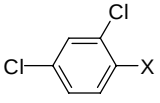	59.4	3.04					3.66
	54.4	2.29					3.35
	58.9	2.67					3.16
8 fragments	80.4	4.17					2.66
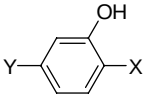	48.5	1.59	6.6	0.93			3.49
	40.7	0.56	6.6	0.93			3.47
	40.7	0.56	7.5	0.08			3.23
4 fragments	48.5	1.59	7.5	0.08			3.18
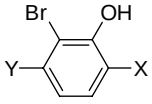	48.5	1.59	6.6	0.93			3.45
1 fragment							
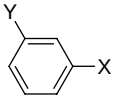	75.0	1.61	8.9	−0.09			3.34
	64.4	3.79	5.5	0.61			2.66
	64.4	3.79	7.7	0.33			2.24
	54.4	2.29	2.6	0.13			2.03
5 fragments	54.4	2.29	5.6	1.02			1.99

(*continued on next page*)

Table 5 (*continued*)

Submolecule[a]	R_X	H_X	R_Y	H_Y	R_Z	H_Z	W_{jl}
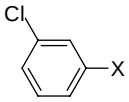 3 fragments	64.4 59.4 54.4	3.79 3.04 2.29					3.23 3.16 2.85
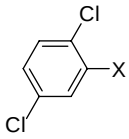 1 fragment	54.4	2.29					3.21
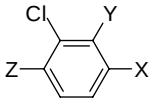 1 fragment	48.5	1.59	2.6	0.13	6.6	0.93	3.07
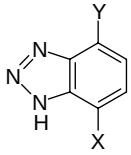 1 fragment	48.5	1.59	6.6	0.93			3.01
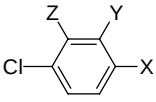 6 fragments	48.5 48.5 50.7 48.5	1.59 1.59 2.05 1.59	2.6 2.6 2.6 2.6	0.13 0.13 0.13 0.13	9.0 6.6 18.6 26.3	−0.53 0.93 −1.31 −1.16	2.93 2.77 2.29 2.25
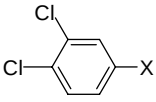 1 fragment	54.4	2.29					2.84
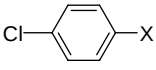 2 fragments	54.4 64.4	2.29 3.79					2.83 2.78
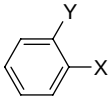 3 fragments	54.4 54.4 54.4	2.29 2.29 2.29	5.5 7.7 2.6	0.61 0.33 0.13			2.83 2.62 2.39
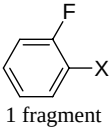 1 fragment	54.4	2.29					2.75
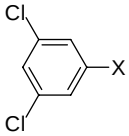 1 fragment	54.4	2.29					2.56
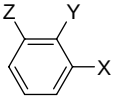 2 fragments	40.7 7.5	0.56 0.08	2.6 40.7	0.13 0.56	7.5 2.6	0.08 0.13	2.56 2.48

Table 5 (*continued*)

Submolecule[a]	R_X	H_X	R_Y	H_Y	R_Z	H_Z	W_{jl}
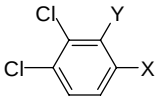	48.5	1.59	2.6	0.13			2.40
1 fragments							
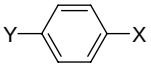	54.4	2.29	5.5	0.61			2.39
	54.4	2.29	5.6	1.02			2.23
6 fragments	64.4	3.79	7.7	0.33			1.84
	54.4	2.29	7.7	0.33			1.83
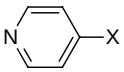	54.4	2.29					2.25
1 fragment							
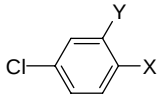	48.5	1.59	2.6	0.13			2.15
1 fragment							
	115.1	2.94					0.73
	54.4	2.29					0.65
2 fragments							
	54.4	2.29					0.57
1 fragment							
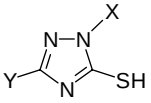	29.3	1.59	25.9	1.61			0.37
38 fragments	29.3	1.59	5.5	0.61			0.36
	55.4	3.46	34.9	3.15			0.16
	29.3	1.59	34.9	3.15			0.15
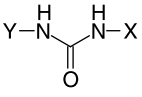	49.0	0.86	34.9	3.15			0.30
	39.1	3.13	32.7	2.69			0.27
	32.0	2.35	24.9	1.66			0.23
17 fragments	31.4	2.35	32.7	2.69			0.23
CH_3–X	54.4	2.29					0.03
	49.9	2.36					0.03
15 fragments	90.4	5.66					0.00
	118.6	3.31					0.00
CF_3–X	78.2	3.77					0.00
3 fragments							
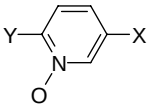	35.8	1.43	34.2	0.23			−0.06
	35.8	1.43	22.8	−0.23			−0.08
	35.8	1.43	42.2	0.82			−0.16
	35.8	1.43	37.7	0.89			−0.17
8 fragments							
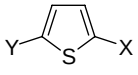	90.5	2.16	25.7	1.22			−0.06
1 fragment							

[a] Selected fragments of each type with minimal and maximal W_{jl} values are presented.

Table 6. Structures and biological activities of the *N*,*N*′-diphenylureas investigated

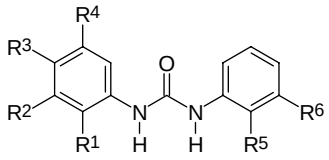

1–17

Compound	R^1	R^2	R^3	R^4	R^5	R^6	IC_{50} (nM)	pIC_{50}
1	OH	H	Cl	H	Br	H	906	6.043
2	OH	Cl	Cl	H	Br	H	63	7.201
3	OH	$CONH_2$	Cl	H	Br	H	10	8.000
4	OH	CH_2NH_2	Cl	H	Br	H	114[a]	6.943
5	OH	SO_2NH_2	Cl	H	Br	H	7	8.155
6	OH	SO_2NMe_2	Cl	H	Br	H	12	7.921
7	OH	H	CN	H	Br	H	25	7.602
8	OH	Br	CN	H	Br	H	6	8.222
9	OH	Cl	CN	H	Br	H	22	7.658
10	OH	CN	Cl	H	Br	H	57	7.244
11	OH	H	NO_2	H	Br	H	22	7.658
12	OH	H	NO_2	H	H	H	320	6.495
13	OH	NO_2	H	H	H	H	860	6.066
14	OH	H	H	NO_2	H	H	10900	4.963
15	OH	H	CN	H	H	H	200	6.699
16	OH	SO_2NH_2	Cl	H	Cl	Cl	9.3	8.032
17	–N=N–NH–		CN	H	Br	H	39	7.495

[a] Solution of compound **4** in the form of hydrochloride was investigated experimentally.

Table 7. Structures and biological activities of the nicotinamide *N*-oxides investigated

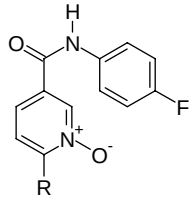

18–25

Compound	R	IC_{50} (nM)	pIC_{50}
18	$–SO_2CH_3$	130	6.886
19	$–SO_2C_2H_5$	130	6.886
20	$–SO_2CH(CH_3)_2$	400	6.398
21	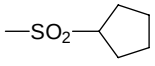	460	6.337
22	$–SO_2C_6H_5$	90	7.046
23	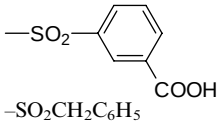	32	7.495
24	$–SO_2CH_2C_6H_5$	280	6.553
25	Cl	1000	6.000

factor in this approach. Regarding Set 1 and Set 2 of the CXCR2 antagonists as a series of parent compounds, while refractions and hydrophobicities are considered recognition parameters, we calculated W_{jl} for submolecules with the use of OS arrays obtained by construction of corresponding base QSAR models. Selected values of W_{jl} minimal and maximal for each type of submolecule are presented in Table 5, together with substituent refractions R and hydrophobicities H in the structures of parent compounds.

The procedure of de novo design can be performed through linking submolecules to one another to achieve the large sum of W_{jl} in a novel molecule.[42,34] The latter should reflect an optimal environment for each fragment which would be close to that in parent molecules. This

Table 8. Structures and biological activities of the quinoxalines investigated

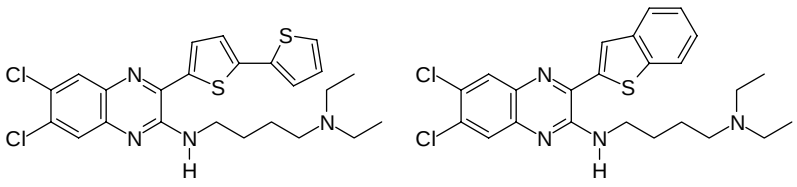

26 **27**

Compound	IC_{50} (nM)	pIC_{50}
26	160	6.796
27	30	7.553

Table 9. Structures and biological activities of the triazolethiols investigated

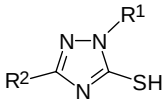

28–59

Compound	R^1	R^2	IC_{50} (nM)	pIC_{50}
28	$C_6H_5CH_2$	C_6H_5	2400	5.620
29	C_6H_5	C_6H_5	Not active	—
30	CH_3	C_6H_5	Not active	—
31	4-$CF_3C_6H_4CH_2$	C_6H_5	Not active	—
32	3-$OHC_6H_4CH_2$	C_6H_5	4400	5.357
33	$C_6H_5CH_2$	4-Pyridinyl	7700	5.114
34	$C_6H_5CH_2$	2-Furanyl	4200	5.377
35	$C_6H_5CH_2$	4-CNC_6H_4	3500	5.456
36	$C_6H_5CH_2$	3-$CF_3C_6H_4$	3500	5.456
37	$C_6H_5CH_2$	4-$CF_3C_6H_4$	2800	5.553
38	$C_6H_5CH_2$	4-$CH_3OC_6H_4$	2300	5.638
39	$C_6H_5CH_2$	3,5-diClC_6H_3	2000	5.699
40	$C_6H_5CH_2$	2-Thienyl	2000	5.699
41	$C_6H_5CH_2$	2-$CH_3C_6H_4$	1400	5.854
42	$C_6H_5CH_2$	2-$CH_3OC_6H_4$	1400	5.854
43	$C_6H_5CH_2$	3-ClC_6H_4	1000	6.000
44	$C_6H_5CH_2$	2-FC_6H_4	890	6.051
45	$C_6H_5CH_2$	4-ClC_6H_4	830	6.081
46	$C_6H_5CH_2$	3,4-diClC_6H_3	800	6.097
47	$C_6H_5CH_2$	2,5-diClC_6H_3	670	6.174
48	$C_6H_5CH_2$	2-ClC_6H_4	450	6.347
49	$C_6H_5CH_2$	2,4-diClC_6H_3	410	6.387
50	$C_6H_5CH_2$	2-BrC_6H_4	350	6.456
51	$C_6H_5CH_2$	2,3-diClC_6H_3	350	6.456
52	4-$CH_3OC_6H_4CH_2$	2,4-diClC_6H_3	10,000	5.000
53	3-$CH_3OC_6H_4CH_2$	2,4-diClC_6H_3	4200	5.377
54	3-$CH_3C_6H_4CH_2$	2,4-diClC_6H_3	730	6.137
55	$C_6H_5CH_2CH_2$	2,4-diClC_6H_3	450	6.347
56	4-$ClC_6H_4CH_2$	2,4-diClC_6H_3	300	6.523
57	3-$C_6H_5OC_6H_4CH_2$	2,4-diClC_6H_3	170	6.770
58	3-$ClC_6H_4CH_2$	2,4-diClC_6H_3	92	7.036
59	3-$ClC_6H_4CH_2$	2-ClC_6H_4	28	7.553

procedure suggests that not only fragments with large W_{jl} are useful for drug design. Some submolecules possess low weights W_{jl} or are flexible ($W_{jl} = 0$). Nevertheless, they may act as good property modifiers to provide a more optimal environment for other fragments. For example, weights of carbamide or triazole fragments are not very high, but apparently they are key submolecules that form certain spatial arrangements and significantly influence the environment of other constituents of molecules. Thus, in future studies, it will be interesting to perform de novo design of CXCR2 antagonists on the base of data from Table 5.

The present model was built on experimental data reflecting competitive interaction between CXCR2, expressed in isolated cellular membranes, and its synthetic

antagonists. However, chemokine receptor activity in living cells is regulated at multiple levels, and CXCR2 antagonists can be also generated based upon secondary binding determinants.[38,39] For example, CXCR2 antagonists, such as Repertaxin, may block CXCR2 via non-competitive allosteric inhibition.[40] Importantly, the frontal polygon method used here could be classified as 'indirect' QSAR approach[35] and would be useful as a tool for structure-based design of drugs with non-competitive mechanisms of action, as well as for QSAR modeling receptor antagonists functionally tested in high throughput screening.

In summary, we applied the frontal polygon method to QSAR analysis of four structural types of CXCR2 antagonists. This method is based on determining local 3D similarity of molecules and uses both geometric and physicochemical parameters of molecular recognition. From the QSAR models that we have obtained, it is apparent that charge distribution is an important factor for inhibition of CXCR2 by small nonpeptide antagonists. Additionally, structural fragments responsible for antagonist activity were identified. This QSAR method provides a relatively accurate model to evaluate biological activities of new CXCR2 antagonists. Furthermore, it is possible that this approach could be further developed for de novo design of novel antagonists.

4. Materials and methods

4.1. Dataset and molecular structures

In this study, 59 CXCR2 antagonists were utilized to construct QSAR models using published biological data.[14,17–22] Four main classes of substances represented in the dataset are *N*,*N*′-diphenylureas, nicotinamide *N*-oxides, quinoxalines, and triazolethiols. The structures of the compounds investigated and their biological activities are shown in Tables 6–9. In these publications, the binding affinity was expressed as an IC_{50} value for [^{125}I]-IL-8 binding to human recombinant CXCR2 expressed in membranes of Chinese hamster ovary cells,[14,17,21,22] BHK-570 cells,[18] and HEK 293 cells.[20] The negative logarithm of IC_{50} value [pIC_{50} or $-\log(IC_{50})$] was adopted as a dependent variable in the QSAR analyses, with the IC_{50} values expressed in molar (M) units.

In order to solve the problem of conformational flexibility, we subdivided the molecules into rigid and flexible fragments (submolecules), as described previously.[32] Phenyl groups, together with monoatomic substituents (halogens), thienyl, benzothienyl, benzodiazine, triazole, benzotriazole rings, as well as methyl and trifluoromethyl groups were treated as rigid fragments. All other submolecules, containing internal rotational degrees of freedom or too small for local similarity analysis, were treated as flexible. The N-C(O)-N group in diphenylureas (without hydrogen atoms) was also considered to be rigid. Local similarity was investigated between peripheral areas (fingerprints) of rigid fragments only, and the flexible fragments did not serve as sources of fingerprints. An example of subdividing compound **16** into rigid and flexible submolecules is shown in Figure 3. Since benzotriazole (compound **17**) may exist in two tautomeric forms, we considered one tautomer as dominant because of the intramolecular hydrogen bond (Fig. 4).

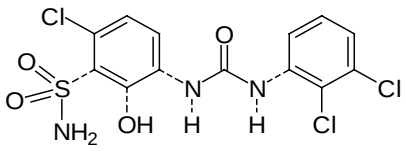

Figure 3. Schematic representation of submolecules of compound **16**. Connections between fragments are shown by dashed lines. The carbamide submolecule and benzene rings plus chlorine atoms form rigid fragments. The remaining fragments (H, OH, SO_2NH_2) are considered 'flexible.'

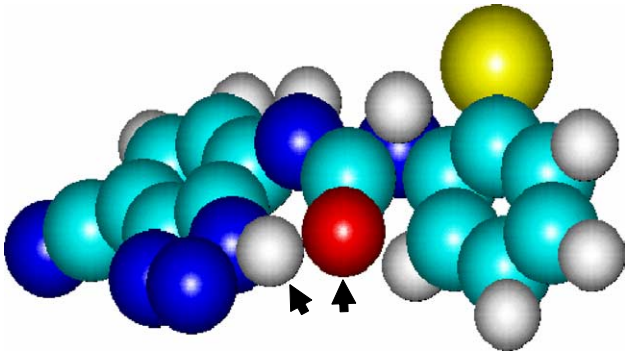

Figure 4. Conformation of compound **17** stabilized by intramolecular hydrogen bonding. Hydrogen bonding between the triazole hydrogen and carbamide oxygen (distance 2.54 Å) stabilized the conformation (arrowheads). The geometry was optimized by the PM3 method (see Section 4.1.1).

The general set of CXCR2 antagonists **1**–**59** was subdivided into two datasets. The first of these (Set 1) included compounds **1**–**27** (diphenylureas, *N*-oxides, and quinoxalines). Set 2 included triazolethiol-derived compounds (**28**–**59**) only, which were taken from publication by Baxter et al.,[20] where the binding activities of the antagonists were determined by the same method. QSAR models were derived for both datasets. In addition, all the antagonists (**1**–**59**) were treated as one set of compounds (Set 1+2), and the corresponding total QSAR models were also constructed.

4.1.1. Conformational analysis. The geometric structures of molecules and atomic charges (q_X) were calculated by a semiempirical PM3 method, as implemented in the HyperChem™ program package (Version 7). Full optimization of geometry was made by the conjugate gradient procedure until the rms gradient became less than 0.01 kcal mol^{-1} Å^{-1}. Atomic coordinates and charges obtained were used for similarity analysis by the frontal polygon method. Other molecular features necessary for this analysis were hydrophobicities (H_X) and molar refractions (R_X) of the corresponding substituents at atoms X. Hydrophobicities and refractions were

calculated by an additive scheme[41] that includes various increments for different atom types and is well suited for compounds **1**–**59**.

4.2. Method of frontal polygons

The frontal polygon method considers the three-dimensional (3D) similarity of molecules, making it possible to process series of conformationally flexible and structurally diverse compounds.[31,32] This method has been extensively characterized and tested previously.[32,42] The frontal polygon method is based on the hypothesis of local 3D similarity, according to which the presence of similar sites on the 'peripheral surface' of molecules makes them close in biological action.[31] It is implied that for complementarity, the ligands must be locally similar to the receptor in terms of geometry, charge distribution, hydrophobic characteristics of atoms, and atomic refractions.

Template molecules for structure comparison were chosen distinctly for each set. Three each of the most active and the least active compounds were used for obtaining template fingerprints (**1**, **5**, **8**, **14**, **16**, **25** within Set 1; **29**–**31**, **57**–**59** within Set 2; **5**, **8**, **16**, **29**–**31** within Set 1+2). Triazines **29**–**31** are inactive, and their pIC_{50} are undefined. These molecules served only as sources of template fingerprints and were not accounted for as data points in QSAR regressions.

The fingerprints obtained from rigid fragments using the approach and parameters proposed previously[31,32] include the projections of atoms characterized by their distances (h_X) to the parent atom X, with the atomic charge (q_X). Projections of the boundary atoms (adjacent to other fragments) were additionally characterized by the hydrophobicities (H_X) and the molar refractions (R_X) of the corresponding substituents at atom X (see Section 4.1.1).

The fingerprints of the CXCR2 antagonist were subjected to a pairwise comparison with template fingerprints to establish the degree of local similarity of molecules in optimal superimpositions (OS), using the following optimality criterion:[31,43]

$$F = \frac{1}{n_0^{\alpha}}\left[w_r \sum r_{XP}^2 + w_h \sum (h_X - h_P)^2 + w_q \sum (q_X - q_P)^2 + w_H \sum (H_X - H_P)^2 + w_R \sum (R_X - R_P)^2\right], \quad (1)$$

where n_0 is the number of assignments in a given OS; $\alpha = 1.5$ is the parameter reflecting the specificity of the superimposition (increasing with n_0); P is the atom from a template molecule fingerprint and X is the atom from a given molecule fingerprint assigned to each other in a given superimposition; r_{XP} is the distance (in Å) between assigned projections in a given superimposition; H_X, H_P are hydrophobicities and R_X, R_P are molar refractions of substituents connected with the atoms X and P (if no submolecules are connected with an atom, then these values are equal to 0); and w_r, w_h, w_q, w_H, and w_R are the weight coefficients. Weight coefficient values were adopted to be reciprocal to dispersions of the molecular recognition criteria r_X, h_X, q_X, H_X, and R_X among all the compounds under consideration. Taking into account that five criteria were used, each weight was calculated as follows:

$$w = 1/(5D), \quad (2)$$

where D is the dispersion of the corresponding criterion. Summation in expression Eq. 1 was performed over the pairs of projections (for atoms X, P) related by assignments. Superimpositions satisfying the conditions:

$$n_0 \geqslant N_0; \quad F \leqslant K_0, \quad (3)$$

(where K_0 and N_0 are parameters) were considered as optimal.

An example of a superimposition and general scheme of the frontal polygon method are shown in Figure 5. Projection of an atom from the superimposed fingerprint is regarded as assigned to a projection from the template fingerprint if the distance between these projections is $\leqslant$0.45 Å.[31,32] Optimality of a superimposition was at-

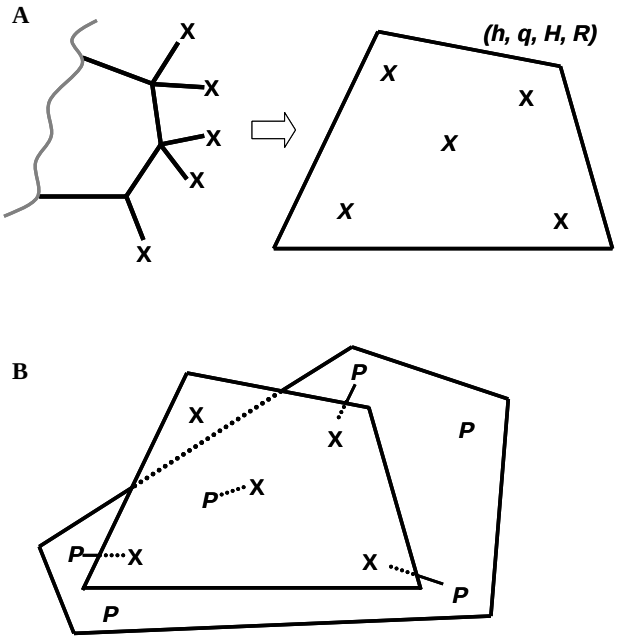

Figure 5. Main steps of structure encoding and local similarity determination for the frontal polygon method. (A) Structure representation. For method applicability to a series of molecules with different sizes and shapes, the 3D-structures of compounds are described in terms of local 3D-similarity. Sets of peripheral atoms (X) lying approximately in the same plane are located in each molecule, and projections of the atoms on the corresponding plane form a fingerprint. Each projection is characterized by the distance h of an atom from the plane and by atomic properties q, H, R. Thus, the 3D-structure of a molecule is encoded by a sequence of the fingerprints. (B) Determining similarity. For determining similarity between molecules, a search of optimal superimpositions (OS) is performed. The fingerprint of a given molecule is translated and rotated in the same plane with the fingerprint of a template molecule to achieve OS with minimal F value. All OS of given molecule fingerprints on all the template fingerprints form an array for calculation of the **V** matrix.

tained by mutual translations and rotations of fingerprints with the use of the efficient algorithm.[43]

QSAR models were constructed using the arrays of OS determined with $N_0 = 4$ (the value recommended in previous publications using the frontal polygon method[31,32,43]) and for various K_0 (i.e., for different requirements on the degree of structural similarity between molecules). Then, the values of K_0 corresponding to the best (base) model were fixed, the weighting coefficients w_q, w_H, and w_R were varied (relative to the values calculated initially from Eq. 2), and new modified QSAR models were constructed in order to assess the role of electron density, hydrophobicity, and substituent volume in the manifestation of a CXCR2 binding affinity.

Finally, particular structure–activity relationships were established in the form of linear equations based on the arrays of OS:

$$\mathrm{pIC}_{50}^{(c)} = \sum_{h=1}^{H} \alpha_h Z_h, \tag{4}$$

where $\mathrm{pIC}_{50}^{(c)}$ is the calculated biological activity and α_h are the regression coefficients. The reduced basis of variables (Z_h) was determined by partial least squares,[33] as described previously.[32] The dimensionality H of the basis was selected as small as possible but still providing for sufficiently high values of the correlation coefficient (R) and the cross-validation coefficient (R_{cv}^2). The latter characterizes the quality of the biological activity prediction in a leave-one-out procedure

$$R_{cv}^2 = 1 - \frac{S_{cv}^2}{S_{ser}^2}, \tag{5}$$

where S_{cv}^2 is the mean-square uncertainty of the prognosis and S_{ser}^2 is the mean-square deviation of activity in the series of compounds studied.

A special feature of the frontal polygon method is the possibility of representing the biological effect of a given compound by the sum of partial effects (weights W_{jl}) related to the component rigid submolecules[32]:

$$\sum_{l=1}^{L} W_{jl} = \mathrm{pIC}_{50,j}^{(c)}, \tag{6}$$

where L is the total number of rigid fragments in the jth molecule. Data on the weights W_{jl} can be useful for the de novo design of active antagonists, as demonstrated recently in the design and synthesis of novel cytochrome P450 ligands.[34] In this study, W_{jl} characteristics were used to assess the extent to which the environment of each fragment determines antagonist binging with CXCR2.

Acknowledgments

This work was supported in part by Department of Defense Grant W9113M-04-1-0001, NIH Grant RR020185 from the National Center for Research Resources, and the Montana State University Agricultural Experimental Station. The U.S. Army Space and Missile Defense Command, 64 Thomas Drive, Frederick, MD 21702, is the awarding and administering acquisition office. The content of this report does not necessarily reflect the position or policy of the U.S. Government.

References and notes

1. Van Haastert, P. J.; Devreotes, P. N. *Nat. Rev. Mol. Cell Biol.* **2004**, *5*, 626.
2. Moser, B.; Wolf, M.; Walz, A.; Loetscher, P. *Trends Immunol.* **2004**, *25*, 75.
3. Murphy, P. M.; Baggiolini, M.; Charo, I. F.; Hebert, C. A.; Horuk, R.; Matsushima, K.; Miller, L. H.; Oppenheim, J. J.; Power, C. A. *Pharmacol. Rev.* **2000**, *52*, 145.
4. Charo, I. F.; Taubman, M. B. *Circ. Res.* **2004**, *95*, 858.
5. Rudolph, E. H.; Woods, J. M. *Curr. Pharm. Des.* **2005**, *11*, 613.
6. Strieter, R. M.; Belperio, J. A.; Burdick, M. D.; Keane, M. P. *Curr. Drug Targets Inflamm. Allergy* **2005**, *4*, 23.
7. Keane, M. P.; Belperio, J. A.; Xue, Y. Y.; Burdick, M. D.; Strieter, R. M. *J. Immunol.* **2004**, *172*, 2853.
8. Proudfoot, A. E. *Nat. Rev. Immunol.* **2002**, *2*, 106.
9. Baggiolini, M. *J. Intern. Med.* **2001**, *250*, 91.
10. Lax, P.; Limatola, C.; Fucile, S.; Trettel, F.; Di, B. S.; Renzi, M.; Ragozzino, D.; Eusebi, F. *J. Neuroimmunol.* **2002**, *129*, 66.
11. Liehn, E. A.; Schober, A.; Weber, C. *Arterioscler. Thromb. Vasc. Biol.* **2004**, *24*, 1891.
12. Hall, L. R.; Diaconu, E.; Patel, R.; Pearlman, E. *J. Immunol.* **2001**, *166*, 4035.
13. Del Rio, L.; Bennouna, S.; Salinas, J.; Denkers, E. Y. *J. Immunol.* **2001**, *167*, 6503.
14. White, J. R.; Lee, J. M.; Young, P. R.; Hertzberg, R. P.; Jurewicz, A. J.; Chaikin, M. A.; Widdowson, K.; Foley, J. J.; Martin, L. D.; Griswold, D. E.; Sarau, H. M. *J. Biol. Chem.* **1998**, *273*, 10095.
15. Auten, R. L.; Richardson, R. M.; White, J. R.; Mason, S. N.; Vozzelli, M. A.; Whorton, M. H. *J. Pharmacol. Exp. Ther.* **2001**, *299*, 90.
16. Lane, B. R.; Lore, K.; Bock, P. J.; Andersson, J.; Coffey, M. J.; Strieter, R. M.; Markovitz, D. M. *J. Virol.* **2001**, *75*, 8195.
17. Cutshall, N. S.; Ursino, R.; Kucera, K. A.; Latham, J.; Ihle, N. C. *Bioorg. Med. Chem. Lett.* **2001**, *11*, 1951.
18. Podolin, P. L.; Bolognese, B. J.; Foley, J. J.; Schmidt, D. B.; Buckley, P. T.; Widdowson, K. L.; Jin, Q.; White, J. R.; Lee, J. M.; Goodman, R. B.; Hagen, T. R.; Kajikawa, O.; Marshall, L. A.; Hay, D. W.; Sarau, H. M. *J. Immunol.* **2002**, *169*, 6435.
19. Li, J. J.; Carson, K. G.; Trivedi, B. K.; Yue, W. S.; Ye, Q.; Glynn, R. A.; Miller, S. R.; Connor, D. T.; Roth, B. D.; Luly, J. R.; Low, J. E.; Heilig, D. J.; Yang, W.; Qin, S.; Hunt, S. *Bioorg. Med. Chem.* **2003**, *11*, 3777.
20. Baxter, A.; Bent, J.; Bowers, K.; Braddock, M.; Brough, S.; Fagura, M.; Lawson, M.; McInally, T.; Mortimore, M.; Robertson, M.; Weaver, R.; Webborn, P. *Bioorg. Med. Chem. Lett.* **2003**, *13*, 4047.
21. Jin, Q.; Nie, H.; McCleland, B. W.; Widdowson, K. L.; Palovich, M. R.; Elliott, J. D.; Goodman, R. M.; Burman, M.; Sarau, H. M.; Ward, K. W.; Nord, M.; Orr, B. M.; Gorycki, P. D.; Busch-Petersen, J. *Bioorg. Med. Chem. Lett.* **2004**, *14*, 4375.
22. Widdowson, K. L.; Elliott, J. D.; Veber, D. F.; Nie, H.; Rutledge, M. C.; McCleland, B. W.; Xiang, J. N.; Jurewicz, A. J.; Hertzberg, R. P.; Foley, J. J.; Griswold,

D. E.; Martin, L.; Lee, J. M.; White, J. R.; Sarau, H. M. *J. Med. Chem.* **2004**, *47*, 1319.
23. Godden, J. W.; Stahura, F. L.; Bajorath, J. *J. Med. Chem.* **2004**, *47*, 5608.
24. Debnath, A. K. *J. Med. Chem.* **2003**, *46*, 4501.
25. Song, M.; Breneman, C. M.; Sukumar, N. *Bioorg. Med. Chem.* **2004**, *12*, 489.
26. Xu, Y.; Liu, H.; Niu, C.; Luo, C.; Luo, X.; Shen, J.; Chen, K.; Jiang, H. *Bioorg. Med. Chem.* **2004**, *12*, 6193.
27. Moitessier, N.; Henry, C.; Maigret, B.; Chapleur, Y. *J. Med. Chem.* **2004**, *47*, 4178.
28. Loew, G. H.; Villar, H. O.; Alkorta, I. *Pharm. Res.* **1993**, *10*, 475.
29. Vedani, A.; Dobler, M.; Dollinger, H.; Hasselbach, K. M.; Birke, F.; Lill, M. A. *J. Med. Chem.* **2005**, *48*, 1515.
30. Liu, J.; Pan, D.; Tseng, Y.; Hopfinger, A. J. *J. Chem. Inf. Comput. Sci.* **2003**, *43*, 2170.
31. Khlebnikov, A. I. *Khim. Farm. Zhurn.* **1994**, *11*, 32.
32. Khlebnikov, A. I. *Khim. Farm. Zhurn.* **1997**, *3*, 41.
33. Glen, W. G.; Dunn, W. J., III *Tetrahedron Comput. Methodol.* **1989**, *2*, 349.
34. Khlebnikov, A. I.; Akhmedzhanov, R. R.; Naboka, O. I.; Bakibaev, A. A.; Tartynova, M. I.; Novozheeva, T. P.; Saratikov, A. S. *Khim. Farm. Zhurn.* **2005**, *1*, 19.
35. Khlebnikov, A.; Schepetkin, I.; Kwon, B. S. *Cancer Biother. Radiopharm.* **2002**, *17*, 193.
36. Gomez-Jeria, J. S.; Morales-Lagos, D. R. *J. Pharm. Sci.* **1984**, *73*, 1725.
37. Ruiz, J.; Lopez, M.; Mila, J.; Lozoya, E.; Lozano, J. J.; Pouplana, R. *J. Comput. Aided Mol. Des.* **1993**, *7*, 183.
38. Jones, S. A.; Dewald, B.; Clark-Lewis, I.; Baggiolini, M. *J. Biol. Chem.* **1997**, *272*, 16166.
39. Kenakin, T. *Receptors Channels* **2004**, *10*, 51.
40. Casilli, F.; Bianchini, A.; Gloaguen, I.; Biordi, L.; Alesse, E.; Festuccia, C.; Cavalieri, B.; Strippoli, R.; Cervellera, M. N.; Di, B. R.; Ferretti, E.; Mainiero, F.; Bizzarri, C.; Colotta, F.; Bertini, R. *Biochem. Pharmacol.* **2005**, *69*, 385.
41. Ghose, A. K.; Crippen, G. M. *J. Med. Chem.* **1985**, *28*, 333.
42. Khlebnikov, A. I.; Naboka, O. I.; Akhmedzhanov, R. R.; Novozheeva, T. P.; Saratikov, A. S. *Khim. Farm. Zhurn.* **1998**, *7*, 35.
43. Khlebnikov, A. I. *Zhurn. Strukt. Khim.* **1995**, *36*, 1083.